

# Coupling of the $A_{1g}$ As-phonon to magnetism in iron pnictides

N.A. García-Martínez,<sup>1</sup> B. Valenzuela,<sup>1</sup> S. Ciuchi,<sup>2,3</sup> E. Cappelluti,<sup>3,1</sup> M.J. Calderón,<sup>1</sup> and E. Bascones<sup>1</sup>

<sup>1</sup>*Instituto de Ciencia de Materiales de Madrid, ICMM-CSIC, Cantoblanco, E-28049 Madrid (Spain).*

<sup>2</sup>*Dipartimento di Scienze Fisiche e Chimiche*

*Università dell'Aquila, CNISM and Istituto Sistemi Complessi CNR, via Vetoio, I-67010 Coppito-L'Aquila (Italy)*

<sup>3</sup>*Istituto de Sistemi Complessi, U.O.S. Sapienza, CNR, v. dei Taurini 19, 00185 Roma, Italy.*

(Dated: June 15, 2021)

Charge, spin and lattice degrees of freedom are strongly entangled in iron superconductors. A neat consequence of this entanglement is the behavior of the  $A_{1g}$  As-phonon resonance in the different polarization symmetries of Raman spectroscopy when undergoing the magneto-structural transition. In this work we show that the observed behavior could be a direct consequence of the coupling of the phonons with the electronic excitations in the anisotropic magnetic state. We discuss this scenario within a five orbital tight-binding model coupled to phonons via the dependence of the Slater-Koster parameters on the As position. We identify two qualitatively different channels of the electron-phonon interaction: a geometrical one related to the Fe-As-Fe angle  $\alpha$  and another one associated with the modification upon As displacement of the Fe-As energy integrals  $pd\sigma$  and  $pd\pi$ . While both mechanisms result in a finite  $B_{1g}$  response, the behavior of the phonon intensity in the  $A_{1g}$  and  $B_{1g}$  Raman polarization geometries is qualitatively different when the coupling is driven by the angle or by the energy integral dependence. We discuss our results in view of the experimental reports.

PACS numbers: 74.70.Xa, 63.20.Kd, 74.25.nd, 74.25.Kc

## I. INTRODUCTION

There is ample experimental evidence that iron pnictides present a rich interplay between charge, lattice and magnetic degrees of freedom. The magnetic transition is commonly accompanied by a structural one. Several phononic spectroscopic signatures show unconventional behavior in the magnetic state.<sup>1–8</sup> At the theoretical level, ab-initio calculations show that the lattice constants and the phonon frequencies depend sensitively on the presence of magnetism,<sup>9,10</sup> and the comparison with experimental measurements is improved when magnetism is included in the calculations.<sup>9,11–15</sup> Furthermore, the electron-phonon coupling has been shown to be enhanced by magnetism.<sup>10,11,16–20</sup> Within this scenario, the role of the spin degree of freedom in the electron-phonon coupling and its possible relevance in the mechanism of superconductivity has been emphasized in several works.<sup>16,18,21,22</sup>

The electronic and magnetic properties are especially sensitive to the height of the pnictogen atom, which affects the band structure at the Fermi level,<sup>23,24</sup> the magnetic moment,<sup>9,16,21,25–27</sup> and possibly the superconducting critical temperature and gap.<sup>28–31</sup> Accordingly, the  $A_{1g}$  As-phonon, which involves vibrations of the As atoms along the c-axis (see Fig. 1) seems to play a special role. Coupling to this phonon has been detected by ultrafast techniques.<sup>32–35</sup> A rapid development of the magnetic ordering upon the vibrational displacement of the  $A_{1g}$  As-phonon has been observed.<sup>32</sup> Features in the ARPES spectrum of 11 compounds with an energy scale close to the one of this phonon have been interpreted in terms of polaron formation.<sup>36</sup>

Raman response represents a powerful tool for inves-

tigating the properties of lattice dynamics.<sup>1,3,5,8,37–43</sup> A significant narrowing of the  $A_{1g}$  As-phonon linewidth at the onset of magnetism has been reported, whereas both softening and hardening of the phonon frequency with decreasing temperature have been observed.<sup>1,39,41</sup> Crucial information is also encoded in the intensity of the phonon resonances. In the undistorted paramagnetic state, the  $A_{1g}$  As-phonon is active neither in the  $B_{1g}$  nor in the  $B_{2g}$  polarization symmetries. When undergoing the magneto-structural transition, a strong phonon signal emerges in the  $B_{1g}$  Raman response but not in  $B_{2g}$ .<sup>8,42</sup> In 122 compounds the  $A_{1g}$  intensity shows a strong enhancement in the magnetic state.<sup>1,3,8,42</sup> On spite of this, in  $\text{BaFe}_2\text{As}_2$  the  $B_{1g}$  intensity is about 1.5 times larger than the  $A_{1g}$  intensity.<sup>8,42</sup> This is not accounted for by the orthorhombic distortion alone, in agreement with the small  $B_{1g}$  Raman intensity observed below the non-magnetic structural transition in  $\text{FeSe}$ .<sup>44</sup>

The aim of this paper is to analyze the unusual Raman response and the changes on the phonon properties in the magnetic state. We show that the dynamical electron-phonon coupling can be responsible for large and unconventional anomalies in the phonon Raman spectrum. We focus on the out-of-plane As lattice vibrations (the  $A_{1g}$  As-phonon) for which we explicitly calculate the electron-phonon coupling within the context of a tight-binding Slater-Koster formalism. The electron-phonon coupling is formally split into two main qualitatively different contributions: *i*) a purely geometrical one ( $\hat{g}^\alpha$ ), related to the variation of the Fe-As-Fe angle  $\alpha$ ; and *ii*) a second one ( $\hat{g}^{pd}$ ) coming from the variation of the Slater-Koster energy integrals  $pd\sigma$  and  $pd\pi$  (see Ref. [24]) upon the modulation of the Fe-As distance. We consider the  $(\pi, 0)$  magnetic state with magnetic moments ordered antiferro-

magnetically in the  $x$  direction and ferromagnetically in the  $y$  direction. Magnetism is included at the mean-field Hartree-Fock level,<sup>45,46</sup> and we study separately its interplay with the sources (i)-(ii) of the electron-phonon interaction. The Raman response is evaluated in the paramagnetic and in the  $(\pi, 0)$  magnetic states using the proper generalization of the charge-phonon theory<sup>47</sup> discussed in Refs. [48,49].

Under generic conditions and excluding any static lattice distortion, the coupling of the phonons with the electronic excitations in the magnetic phase is able by itself to induce a Raman intensity in the  $B_{1g}$  Raman polarization. This is due to the symmetry breaking in the anisotropic magnetic state. Only the electron-phonon coupling  $\hat{g}^\alpha$  accounts for the fact that the  $B_{1g}$  Raman signal can be larger than the  $A_{1g}$  Raman signal, the latter strongly decreasing in the magnetic state. A large enhancement in  $A_{1g}$  with magnetism appears when coupling electrons and phonons via  $\hat{g}^{pd}$ . Based on symmetry considerations, we argue that in the double stripe magnetic order of FeTe the out-of-plane  $A_{1g}$  vibrations of the Te atoms will show finite Raman intensity only within the  $B_{2g}$  polarization set-up and not in the  $B_{1g}$  one. With increasing interactions the phonon frequency softens when entering into the magnetic state but hardening is observed for the  $\hat{g}^{pd}$  coupling for the largest values of the on-site electronic interactions  $U$  considered.

## II. THEORY

### A. Model

The Hamiltonian we use to study the electron-phonon coupling on the Fe superconductors has three terms

$$H = H_0 + H_{ph} + H_U. \quad (1)$$

$H_0$  is the five Fe d-orbital tight-binding model for the Fe-As planes, obtained after eliminating the As degree of freedom and previously proposed in Ref. [24].  $H_{ph}$  is the phonon part including the free phonon and the electron-phonon interaction, and  $H_U$  contains the electronic interactions. The one Fe unit cell is used with  $x$  and  $y$  directions along the nearest neighbor Fe-Fe bonds. In the following we describe in detail each of the terms of the Hamiltonian.

*a. Free electron part.* The band structure of the system is taken into account via the free electron term  $H_0$

$$H_0 = \sum_{\mathbf{k}, \mu, \nu, \sigma, r} F_{\mu\nu}^r(\mathbf{k}) t_{\mu\nu}^r c_{\mathbf{k}\mu\sigma}^\dagger c_{\mathbf{k}\nu\sigma} + \sum_{i, \mu, \sigma} \epsilon_\mu c_{i\mu\sigma}^\dagger c_{i\mu\sigma}, \quad (2)$$

where  $c_{\mathbf{k}\mu\sigma}^\dagger$  creates an electron on the Fe d-orbital  $\mu$  with spin  $\sigma$  and wave vector  $\mathbf{k}$ , and  $c_{i\mu\sigma}^\dagger$  represents the same operator in real space.  $F_{\mu\nu}^r(\mathbf{k})$  is the electronic  $\mathbf{k}$ -dispersion relation<sup>24</sup> and  $\epsilon_\mu$  is the crystal field.  $r$  labels the three different directions for the hoppings  $t_{\mu\nu}^r$ ,

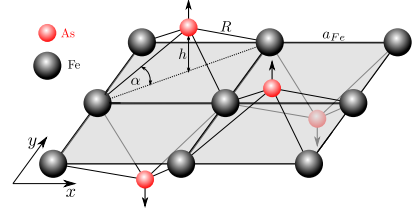


FIG. 1: (Color online) Sketch of the lattice structure showing the  $A_{1g}$  As-phonon in iron arsenides. The Fe-Fe nearest neighbor distance  $a_{Fe}$ , the Fe-As-Fe angle  $\alpha$ , the Fe-As distance  $R$  and the As height with respect to the iron plane  $h$  are indicated.

with different  $\mathbf{k}$ -dispersions, taken into account: between first neighbors in the  $x$ -direction, first neighbors in the  $y$ -direction, and second neighbors.

Direct Fe-Fe hoppings between their d-orbitals and indirect through the As p-orbitals are considered. Indirect hopping is included to second order in perturbation theory.<sup>24</sup> Within the Slater-Koster framework considered,<sup>50</sup> the hopping parameters have explicit information on the geometry of the pnictogen tetrahedra. These parameters depend on  $\alpha$ , the angle between the Fe-As bond and the Fe plane (see Fig. 1) and on the energy integrals. The direct Fe-Fe hoppings depend on the energy integrals  $dd\sigma$ ,  $dd\pi$  and  $dd\delta$  between the Fe d-orbitals while the indirect (through the As) Fe-Fe hoppings depend on  $pd\sigma$  and  $pd\pi$  between the Fe d-orbitals and the As p-orbitals. These energy integrals are a function of the relative distance between the constituent atoms. The analytic expressions for all the hoppings  $t_{\mu\nu}^r$  are given in Ref. [24].

The energy integrals and crystal field  $\epsilon_\mu$  parameters in Eq. (2) are chosen to correctly describe the bands, their orbital compositions, the Fermi surface, and the modification induced by  $\alpha$  as provided by electronic structure calculations. Details are given in Ref. [24].  $H_0$  has *tetragonal* symmetry, i.e. the static orthorhombic distortion found in the magnetic phase is not included in our calculations.

*b. Phonon part.*  $H_{ph}$  is given by

$$H_{ph} = \sum_{\mathbf{q}} \omega_{\mathbf{q}} a_{\mathbf{q}}^\dagger a_{\mathbf{q}} + \sum_{\mathbf{k}, \mathbf{q}, \mu, \nu, \sigma, M} g_{\mu\nu}^M(\mathbf{k}, \mathbf{q}) c_{\mathbf{k}+\mathbf{q}\mu\sigma}^\dagger c_{\mathbf{k}\nu\sigma} (a_{\mathbf{q}} + a_{-\mathbf{q}}^\dagger) \quad (3)$$

where  $a_{\mathbf{q}}^\dagger$  creates a phonon in the  $A_{1g}$  As-mode at wave vector  $\mathbf{q}$ ,  $\omega_{\mathbf{q}}$  is the phonon frequency and  $g_{\mu\nu}^M(\mathbf{k}, \mathbf{q})$  the electron-phonon matrix element between orbitals  $\mu$  and  $\nu$ .  $M$  labels the type of interaction considered. The vertical displacement of the As atoms  $\delta h$  (squeezing and elongating the tetrahedra) gives rise to a modification of  $\alpha$  around the equilibrium position  $\alpha_0$  and to a variation of the energy integrals  $pd\sigma$  and  $pd\pi$  (only the indirect hoppings are affected by this phonon). The two interaction terms that arise are labelled  $\hat{g}^\alpha$  and  $\hat{g}^{pd}$ , namely,

$M = \alpha$  and  $M = pd$  respectively. In each of these cases, the electron-phonon interaction may arise from the variation of the hopping  $t_{\mu\nu}^r$  with phonon coordinates giving rise to *non-local* contributions, and from the variation of the crystal field  $\epsilon_\mu$  resulting in *local* contributions:  $g^M = g^{M,loc} + g^{M,non-loc}$ .

The crystal field  $\epsilon_\mu$  can be decomposed in a term which includes the electrostatic interactions between the ions in the system  $\epsilon_\mu^{Coul}$  and a contribution that depends on the As orbital energies  $\epsilon_\mu^{ind}$ . The dependence of  $\epsilon_\mu^{Coul}$  on the As position is beyond the scope of the present study and is neglected here. We only consider the dependence of  $\epsilon_\mu^{ind}$  (see Appendix A).

The non-local part  $\hat{g}^{\alpha,non-loc}$  involves the derivatives of the hoppings with respect to  $\alpha$  [straightforwardly calculated from  $h$ , the distance between the As atoms and the Fe plane, and  $a_{Fe}$ , the Fe-Fe nearest neighbor distance, as  $\alpha = \arctan(\sqrt{2}h/a_{Fe})$ , see Fig. 1] and a form factor  $\hat{F}_{\mu\nu}^r(\mathbf{k}, \mathbf{q})$  which depends on the symmetry of the lattice and the orbitals. As we are here interested in the Raman response,  $\mathbf{q} = \mathbf{0}$  and  $\hat{F}_{\mu\nu}^r(\mathbf{k}, \mathbf{q}) = F_{\mu\nu}^r(\mathbf{k})$ . In the orbital basis, the  $\hat{g}^{\alpha,non-loc}$  electron-phonon coupling is given by

$$g_{\mu\nu}^{\alpha,non-loc}(\mathbf{k}) = \sum_r F_{\mu\nu}^r(\mathbf{k}) \frac{\partial t_{\mu\nu}^r}{\partial \alpha} \delta\alpha, \quad (4)$$

with  $\delta\alpha = \frac{\partial \alpha}{\partial h} \delta h$  and form factors  $F_{\mu\nu}^r(\mathbf{k})$  as in Eq. (2). Analogously

$$g_{\mu\mu}^{\alpha,loc} = \frac{\partial \epsilon_\mu^{ind}}{\partial \alpha} \delta\alpha. \quad (5)$$

This contribution to the interaction Hamiltonian appears as a constant (non  $\mathbf{k}$ -dependent) diagonal term.

$\hat{g}^{pd}$  involves the derivatives of the hoppings with respect to  $pd\sigma$  and  $pd\pi$ . These integrals are a decaying function of  $R$ , the distance between Fe and As atoms.  $R$  is related to  $h$  as  $R = h/\sin \alpha$ . We assume the  $R$  dependence is the same for both  $pd\sigma$  and  $pd\pi$ :  $pd\sigma = C_{pd\sigma} f(R)$  and  $pd\pi = C_{pd\pi} f(R)$ . If  $R_0$  is the Fe-As distance corresponding to the equilibrium angle  $\alpha_0$ ,  $pd\sigma_0 = C_{pd\sigma} f(R_0)$  and  $pd\pi_0 = C_{pd\pi} f(R_0)$ . Expanding around this equilibrium value  $pd\sigma = pd\sigma_0 \left[1 + \frac{1}{f(R_0)} \frac{\partial f(R)}{\partial R} \delta R\right]$ , and equivalently for  $pd\pi$ . Therefore,  $\delta pd\sigma = pd\sigma_0 \frac{1}{f(R_0)} \frac{\partial f(R)}{\partial R} \frac{\partial R}{\partial h} \delta h$  and  $\delta pd\pi = pd\pi_0 \frac{1}{f(R_0)} \frac{\partial f(R)}{\partial R} \frac{\partial R}{\partial h} \delta h$ . Consequently,  $\delta pd\pi = \frac{pd\pi_0}{pd\sigma_0} \delta pd\sigma$ . Using these relations, in the orbital basis

$$g_{\mu\nu}^{pd,non-loc}(\mathbf{k}) = \sum_r F_{\mu\nu}^r(\mathbf{k}) \delta pd\sigma \left( \frac{\partial t_{\mu\nu}^r}{\partial pd\sigma} + \frac{\partial t_{\mu\nu}^r}{\partial pd\pi} \frac{pd\pi_0}{pd\sigma_0} \right), \quad (6)$$

$$g_{\mu\mu}^{pd,loc} = \delta pd\sigma \left( \frac{\partial \epsilon_\mu^{ind}}{\partial pd\sigma} + \frac{\partial \epsilon_\mu^{ind}}{\partial pd\pi} \frac{pd\pi_0}{pd\sigma_0} \right). \quad (7)$$

Here we take  $f(R) = 1/R^4$ . This dependence is valid assuming the  $p$  and  $d$  orbitals are very localized and they

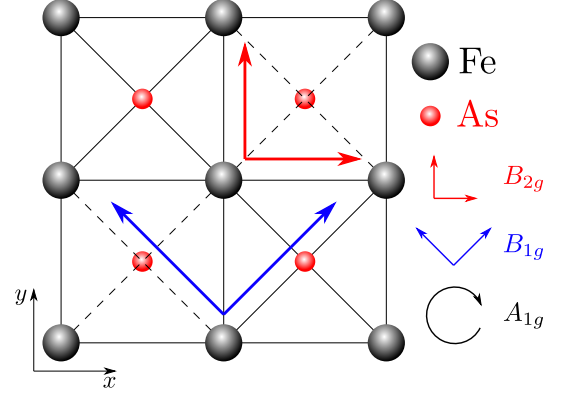


FIG. 2: (Color online)  $A_{1g}$ ,  $B_{1g}$  and  $B_{2g}$  Raman symmetries for the Fe-As layer. We work in the one Fe unit cell with  $x$  and  $y$  directions along the nearest neighbor Fe-Fe bonds.

only couple through plane-wave corrections to the atomic state wave-functions.<sup>51</sup> The pnictides have a strong covalent character that may invalidate the localization assumption, hence this particular functional dependence must be taken with caution. Therefore, a direct quantitative comparison between  $\hat{g}^\alpha$  and  $\hat{g}^{pd}$  would not be reliable, hence we present the results for the two electron-phonon interactions separately.

*c. Correlation part.*  $H_U$  includes the local interactions (intraorbital  $U$ , Hund's coupling  $J_H$  and interorbital  $U' = U - 2J_H$ ) and is treated within Hartree-Fock mean field approximation with focus on the  $(\pi, 0)$  antiferromagnetic state (see Refs. [45,46] for details). The Hartree-Fock self-consistency includes the electronic degrees of freedom and not the phonons. The model without phonons ( $H_0 + H_U$ ) has been previously used to study the magnetic phase diagram as a function of  $U$  and  $J_H/U$  within a Hartree-Fock approximation.<sup>45,46,52</sup> With increasing  $U$  a metallic AF  $(\pi, 0)$  state arises. For a narrow range of values of  $U$ , the system can be described as itinerant, but a strong orbital differentiation develops for larger values of  $U$ .<sup>46</sup> In the orbital differentiated region, the  $3z^2 - r^2$ ,  $x^2 - y^2$  and  $zx$  orbitals are itinerant while  $xy$  and  $yz$  are gapped at half-filling at the Fermi energy. These results are consistent with experimental<sup>53,54</sup> and theoretical<sup>55-58</sup> reports of different renormalization values for the bands depending on their orbital character. In our calculations,<sup>46</sup> for  $J_H/U = 0.25$  the itinerant region occurs for  $1.45 \text{ eV} < U < 1.7 \text{ eV}$  and the orbital differentiation for  $U > 1.7 \text{ eV}$ .

## B. Phonon-mediated Raman scattering theory

Raman scattering measures the total cross section of the inelastic scattering of electrons

$$\frac{\partial^2 \sigma}{\partial \Omega \partial \omega_S} = h r_0^2 \frac{\omega_S}{\omega_I} S(i\Omega \rightarrow \Omega + i0) \quad (8)$$

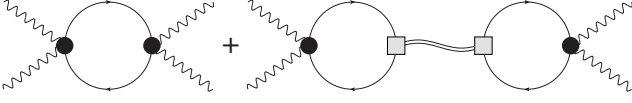


FIG. 3: Electronic Raman diagram (left) and phonon-mediated Raman diagram (right). The wavy line is the photon propagator, the double wavy line is the phonon propagator. The circle stands for the Raman vertex and the square for the electron-phonon interaction, either  $\hat{g}^\alpha$  or  $\hat{g}^{pd}$ . The electronic Raman diagram was studied in Ref. [59].

with  $\omega_I$  and  $\omega_S$  the frequency of the incident and the scattered light respectively and  $r_0$  the Thomson radius. The Raman intensity can be related to the imaginary part of the Raman response function

$$S^\lambda(\Omega) = -\pi^{-1}(1 + n(\Omega, T))\text{Im}\chi^\lambda(\Omega) \quad (9)$$

with  $\lambda = B_{1g}, B_{2g}, A_{1g}$  the symmetries of the squared lattice point group depending on the incident and scattered photon polarizations represented in Fig. 2. The symmetries are defined with the  $x$  and  $y$  axis along the Fe-Fe nearest-neighbors, as in the Hamiltonian. This definition is different from the one used in some experimental papers.<sup>8</sup>

Only non-resonant diagrams are included in the calculation of the Raman response. To study the phonon contribution we use the charge-phonon theory originally proposed by M.J. Rice<sup>47</sup> for the optical conductivity and recently used<sup>48,49</sup> to study the Raman response in graphene. The Raman response includes the diagrams shown in Fig. 3: the electronic bubble contribution  $\chi_{el-el}^\lambda$  (left) and the charge-phonon diagram  $\Delta\chi_{ph}^\lambda$  (right),

$$\chi^\lambda(\Omega) = \chi_{el-el}^\lambda(\Omega) + \Delta\chi_{ph}^\lambda(\Omega). \quad (10)$$

The electronic Raman response  $\chi_{el-el}^\lambda$  was studied in Ref. [59] and is not discussed in this work. Here we concentrate our attention on the phonon-mediated Raman response that can be expressed as a sum on all electron-phonon channels  $M, M'$ :  $\Delta\chi_{ph}^\lambda(\Omega) = \sum_{M, M'} \Delta\chi_{ph, M, M'}^\lambda$ ,

$$\Delta\chi_{ph, M, M'}^\lambda(\Omega) = \chi_M^\lambda(\Omega) D_0(\Omega) \chi_{M'}^{*\lambda}(\Omega), \quad (11)$$

with  $D_0(\Omega) = D_0(\mathbf{q} = 0, \Omega)$  the phonon propagator. To address separately the contribution of a single electron-phonon channel we focus on the diagonal part of  $\Delta\chi_{ph, M, M'}^\lambda = \Delta\chi_{ph, M}^\lambda$ .

In the vicinity of the resonance we can approximate

$$D_0(\Omega) = \frac{1}{(\Omega - \Omega_0) + i\Gamma_0}. \quad (12)$$

with  $\Omega_0$  the phonon frequency and  $\Gamma_0$  the phonon scattering rate.

$\chi_M^\lambda$  is a mixed response which includes both the electron-phonon couplings  $\hat{g}^M$  defined in Eqs. (4)-(5) and (6)-(7) and the Raman vertex  $\gamma^\lambda$ . The  $\gamma^\lambda$  vertices encode

information of the incident and scattered light, and the point group symmetry of the squared lattice.<sup>60</sup> In the orbital basis they are given by:<sup>59</sup>

$$\gamma_{\mu\nu}^{B_{1g}}(\mathbf{k}) = \frac{\partial^2 \epsilon_{\mu\nu}(\mathbf{k})}{\partial k_x^2} - \frac{\partial^2 \epsilon_{\mu\nu}(\mathbf{k})}{\partial k_y^2}, \quad (13)$$

$$\gamma_{\mu\nu}^{B_{2g}}(\mathbf{k}) = \frac{\partial^2 \epsilon_{\mu\nu}(\mathbf{k})}{\partial k_x \partial k_y}, \quad (14)$$

$$\gamma_{\mu\nu}^{A_{1g}}(\mathbf{k}) = \frac{\partial^2 \epsilon_{\mu\nu}(\mathbf{k})}{\partial k_x^2} + \frac{\partial^2 \epsilon_{\mu\nu}(\mathbf{k})}{\partial k_y^2}. \quad (15)$$

Separating real and imaginary parts  $\chi_M^\lambda = \chi_M'^\lambda + i\chi_M''^\lambda$

$$\begin{aligned} \chi_M'^\lambda(\Omega) &= \frac{1}{V} \sum_{\mathbf{k}\sigma n n'} \gamma_{nn'}^\lambda(\mathbf{k}) g_{nn'}^{M*}(\mathbf{k}) (f(E_n(\mathbf{k})) - f(E_{n'}(\mathbf{k}))) \\ &\times \left( \frac{\Omega + E_n(\mathbf{k}) - E_{n'}(\mathbf{k})}{(E_n(\mathbf{k}) - E_{n'}(\mathbf{k}) + \Omega)^2 + \eta^2} \right. \\ &\left. + \frac{-\Omega + E_n(\mathbf{k}) - E_{n'}(\mathbf{k})}{(E_n(\mathbf{k}) - E_{n'}(\mathbf{k}) - \Omega)^2 + \eta^2} \right) \end{aligned} \quad (16)$$

$$\begin{aligned} \chi_M''^\lambda(\Omega) &= -\frac{\pi}{V} \sum_{\mathbf{k}\sigma n n'} \gamma_{nn'}^\lambda(\mathbf{k}) g_{nn'}^{M*}(\mathbf{k}) (f(E_n(\mathbf{k})) - f(E_{n'}(\mathbf{k}))) \\ &\times (\delta(\Omega + E_n(\mathbf{k}) - E_{n'}(\mathbf{k})) - \delta(-\Omega + E_n(\mathbf{k}) - E_{n'}(\mathbf{k}))) \end{aligned} \quad (17)$$

with  $\delta$  functions broadened by  $\eta$ . Here  $V$  is the volume,  $E_n, E_{n'}$  label the energies of the bands  $n$  and  $n'$ ,  $f(E)$  is the Fermi function,  $g_{nn'}^M(\mathbf{k}) = \sum_{\mu\nu} a_{\mu n}^*(\mathbf{k}) g_{\mu\nu}^M(\mathbf{k}) a_{\nu n'}(\mathbf{k})$  and  $\gamma_{nn'}^\lambda(\mathbf{k}) = \sum_{\mu\nu} a_{\mu n}^*(\mathbf{k}) \gamma_{\mu\nu}^\lambda(\mathbf{k}) a_{\nu n'}(\mathbf{k})$  with  $a_{\mu n}$  the matrix which rotates between the orbital and the band basis.<sup>59</sup> The matrix elements  $g_{nn'}^M(\mathbf{k})$  and  $\gamma_{nn'}^\lambda(\mathbf{k})$  determine whether the phonon is Raman active.

$\Delta\chi_{ph, M}^\lambda(\Omega)$  can be rewritten as a function of the phonon intensity  $I_M^\lambda$  and the Fano factor  $q_M^\lambda$  [49]

$$\text{Im}\Delta\chi_{ph, M}^\lambda(\Omega) = -I_M^\lambda \frac{(q_M^\lambda)^2 - 1 + 2(\frac{\Omega - \Omega_0}{\Gamma_0}) q_M^\lambda}{(q_M^\lambda)^2 (1 + (\frac{\Omega - \Omega_0}{\Gamma_0})^2)} \quad (18)$$

with the intensity prefactor  $I_M^\lambda$  and the Fano factor  $q_M^\lambda$  given by

$$I_M^\lambda = \frac{(\chi_M'^\lambda(\Omega_0))^2}{\Gamma_0}, \quad (19)$$

$$q_M^\lambda = -\frac{\chi_M'^\lambda(\Omega_0)}{\chi_M''^\lambda(\Omega_0)}. \quad (20)$$

This formula will be used below to study the symmetry dependence and intensity of the  $A_{1g}$  As-phonon. If  $|q_M^\lambda|$  is large, the phonon signal acquires a symmetric shape. If in Eq. (18) we replace  $\Omega = \Omega_0$ , for  $q_M^\lambda \gg 1$  we find  $\text{Im}\Delta\chi_{ph, M}^\lambda(\Omega_0) = -I_M^\lambda$ . The Raman signal turns out positive when replaced in Eq. (9).

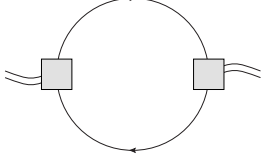


FIG. 4: Phonon self energy. The square stands for the electron phonon interaction: either  $\hat{g}^\alpha$  or  $\hat{g}^{pd}$ .

### C. Phonon self-energy

We study the  $\mathbf{q} = 0$  phonon self-energy contribution  $\Pi_M(\Omega) = \Pi'_M(\Omega) + i\Pi''_M(\Omega)$  arising from the coupling to the electrons. The real part produces a hardening or softening of the phonon and the imaginary part contributes to the phonon broadening. In the second order perturbation theory approximation,<sup>61</sup> (see Fig. 4) the phonon self-energy can be expressed as a sum on all the electron-phonon channels  $M, M'$ :  $\Pi(\Omega) = \sum_{M, M'} \Pi_{ph, M, M'}^\lambda(\Omega)$ . We consider only the diagonal part of the self-energy  $\Pi_M(\Omega)$  for which the real and imaginary part read

$$\begin{aligned} \Pi'_M(\Omega) = & \frac{1}{V} \sum_{\mathbf{k}\sigma n n'} |g_{nn'}^M(\mathbf{k})|^2 (f(E_n(\mathbf{k})) - f(E_{n'}(\mathbf{k}))) \\ & \times \left( \frac{\Omega + E_n(\mathbf{k}) - E_{n'}(\mathbf{k})}{(E_n(\mathbf{k}) - E_{n'}(\mathbf{k}) + \Omega)^2 + \eta^2} \right. \\ & \left. + \frac{-\Omega + E_n(\mathbf{k}) - E_{n'}(\mathbf{k})}{(E_n(\mathbf{k}) - E_{n'}(\mathbf{k}) - \Omega)^2 + \eta^2} \right) \end{aligned} \quad (21)$$

$$\begin{aligned} \Pi''_M(\Omega) = & -\frac{\pi}{V} \sum_{\mathbf{k}\sigma n n'} |g_{nn'}^M(\mathbf{k})|^2 (f(E_n(\mathbf{k})) - f(E_{n'}(\mathbf{k}))) \\ & \times (\delta(\Omega + E_n(\mathbf{k}) - E_{n'}(\mathbf{k})) - \delta(-\Omega + E_n(\mathbf{k}) - E_{n'}(\mathbf{k}))) . \end{aligned} \quad (22)$$

A small broadening  $\eta$ , which also enters in the  $\delta$  functions, has been introduced.

## III. RESULTS

We have calculated the phonon contribution to the Raman response and the correction to the phonon self-energy induced by the electron-phonon coupling in the paramagnetic and  $(\pi, 0)$  antiferromagnetic states at zero temperature. We study the  $A_{1g}$  As-phonon and consider the two electron-phonon couplings introduced in Section II A,  $\hat{g}^\alpha$  and  $\hat{g}^{pd}$ . We choose generic interactions to describe the iron pnictides,  $J_H = 0.25U$  with  $U$  ranging from the paramagnetic phase  $U < 1.45$  eV, through the itinerant magnetic phase  $1.45 \text{ eV} < U < 1.7$  eV to the orbital differentiated region<sup>46</sup>  $U > 1.7$  eV.  $\alpha_0 = 35.3^\circ$  and  $n = 6$ , corresponding to a regular tetrahedra and undoped pnictides, are considered unless otherwise stated. We take  $\delta\hbar = 0.02 \text{ \AA}$ , and  $\Omega_0 = 20 \text{ meV}$  and  $\Gamma_0 = 1$

meV for the phonon frequency and scattering rate (values are similar to the experimental ones<sup>1,39,41</sup>). Within the Hartree-Fock approximation used here to include the local interactions, the renormalization of the bands is not properly accounted for. Comparison of *ab-initio* electronic structure calculations and ARPES measurements render a factor of 3 for the renormalization of the bands. Therefore once the ground state has been obtained, the energy bands are divided by 3 to account for the renormalization observed in ARPES experiments<sup>62</sup> and not reproduced at the Hartree-Fock level.

### A. Raman response

Fig. 5 is the main result of this work. It shows the  $A_{1g}$  and the  $B_{1g}$  phonon Raman intensities due to the couplings  $\hat{g}^\alpha$  (left) and  $\hat{g}^{pd}$  (right). For both couplings  $\hat{g}^M$ , the intensity  $I_M^{A_{1g}}$  in the  $A_{1g}$  polarization is finite in both the paramagnetic and magnetic states while  $I_M^{B_{1g}}$  is finite only in the antiferromagnetic state. The  $B_{2g}$  phonon intensity, not shown, vanishes in all the range of parameters.<sup>63</sup> While  $H_0$  is tetragonal, this symmetry is broken in the anisotropic  $(\pi, 0)$  magnetic state. The  $x$  and  $y$  directions become inequivalent due to the reorganization of the *electronic* degrees of freedom. The  $B_{1g}$  signal is antisymmetric under the  $k_x \rightarrow k_y$  rotation, see Eq. (13), and it is sensitive to  $k_x$  being non equivalent to  $k_y$  in the magnetic state. This sensitivity results in a finite  $I_M^{B_{1g}}$ .  $B_{2g}$ , however, is antisymmetric under either  $k_x \rightarrow -k_x$  or  $k_y \rightarrow -k_y$ , see Eq. (14).  $I_M^{B_{2g}}$  is not sensitive to the breaking of the tetragonal symmetry in the  $(\pi, 0)$  state and remains zero.

A strong change in the intensity is also observed in the  $A_{1g}$  Raman polarization when entering in the magnetic state. The Raman intensity  $I_M^{A_{1g}}$  is related to the real part of the mixed bubble at the phonon frequency  $\chi_M'^{A_{1g}}(\Omega_0)$  via Eq. (19).  $\chi_M'^{A_{1g}}(\Omega_0)$ , Kramers-Krönig integral of  $\chi_M''^{A_{1g}}(\Omega_0)$ , is sensitive to the reorganization of the electronic structure in the magnetic state, especially close to the Fermi level, at energies comparable to  $\Omega_0$ .

The  $A_{1g}$  and the  $B_{1g}$  signals show a qualitatively different behavior for the two different electron-phonon couplings considered:  $\hat{g}^\alpha$  [Fig. 5(a)] and  $\hat{g}^{pd}$  [Fig. 5(b)]. In the magnetic state,  $I_\alpha^{A_{1g}}$  decreases with respect to the intensity in the paramagnetic state, while  $I_{pd}^{A_{1g}}$  increases.  $I_\alpha^{B_{1g}}$  increases in the magnetic state while  $I_{pd}^{B_{1g}}$  shows a bump as a function of  $U$  getting close to zero for  $U = 2$  eV.

The non-local components of the electron-phonon interactions, Eqs. (4) and (6), appear to dominate the qualitative behaviour of the Raman intensity. This can be seen by comparing the total intensities in Fig. 5 with the non-local terms of the mixed bubble  $\chi_M'^\lambda(\Omega_0)$  in Fig. 6 ( $I_M^\lambda$  and  $\chi_M'^\lambda$  are related by Eq. 19). The relevant features shown in the solid lines of Fig. 6 mimic the curves



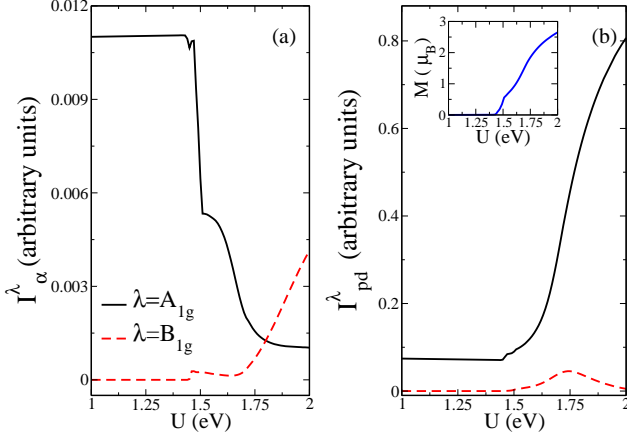


FIG. 5: (Color online)  $A_{1g}$  and  $B_{1g}$  phonon Raman intensities versus the on-site interaction  $U$  for the electron-phonon coupling  $\hat{g}^\alpha$  (a) and  $\hat{g}^{pd}$  (b). Note that in the magnetic state,  $\hat{g}^\alpha$  for  $U > 1.8$  eV shows a bigger  $B_{1g}$  response than the  $A_{1g}$  one, while  $\hat{g}^{pd}$  gives a strong enhancement of the  $A_{1g}$  polarization signal. Inset in (b) Magnetic moment as a function of the interaction  $U$ .  $J_H/U = 0.25$ ,  $\Omega_0 = 20$  meV,  $\delta h = 0.02$  Å,  $\Gamma_0 = 1$  meV, and  $\eta = 3$  meV have been used.

in Fig. 5.

The non-local components  $\chi_M^{\lambda, \text{non-loc}}(\Omega_0)$  result to be a linear combination of the same  $\mathbf{k}$ -dependent form factors  $F_{\mu\nu}^r(\mathbf{k})$  in both  $M = \alpha$  and  $M = pd$  phonon channels. Therefore, for a given photon polarization, the difference in the behaviour of  $\chi_M^\lambda$  and  $I_M^\lambda$  should be ascribed to the difference in the coefficients of the form factors. In order to gain a deeper insight on this issue, we have further decomposed  $\chi_M^{\lambda, \text{non-loc}}(\Omega_0)$  into first and second nearest neighbor contributions. In Fig. 6 we see that the different behaviors observed in the Raman intensity in Fig. 5 for the two electron-phonon couplings as a function of  $U$  are partly a consequence of the fact that in some cases different contributions add up and in other cases subtract.

The Raman intensities are not just a simple function of the magnetic moment (see inset in Fig. 5(b)). Non-monotonic dependences in momentum are frequently found, especially in the itinerant region. This becomes also clear when comparing the spectrum corresponding to different angles  $\alpha_0$ , electron filling  $n$  and interactions (not shown). A change in the electron filling and Fe-As-Fe angle induces changes in the band structure and in the transitions at energies close to  $\Omega_0$  and consequently in the Raman spectrum.

The Fano factors  $q_M^\lambda$ , not shown, corresponding to  $\hat{g}^\alpha$  and  $\hat{g}^{pd}$  are calculated using the expression in Eq. 20. For  $\hat{g}^\alpha$  and for both polarizations  $B_{1g}$  and  $A_{1g}$ , the Fano factor is generally large and negative with values between  $-40$  and  $-30$  for  $U \geq 1.8$  eV. For  $\hat{g}^{pd}$  the Fano factor is even larger and still negative reaching around  $-40$  just for  $1.8 \leq U \leq 1.9$  eV in the  $B_{1g}$  polarization. This Fano factor corresponds to an almost symmetric Lorentzian form of the Raman phonon peak. For smaller values of

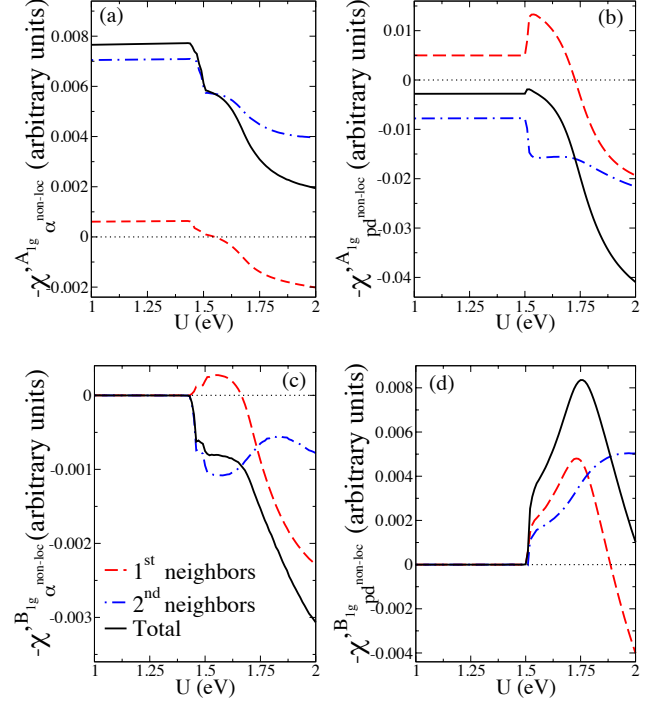


FIG. 6: (Color online) Real part of the non-local terms of the mixed bubble  $\chi_M^\lambda(\Omega_0)$ :  $\chi_{\alpha}^{\lambda, \text{non-loc}}$  (a),  $\chi_{pd}^{\lambda, \text{non-loc}}$  (b),  $\chi_{\alpha}^{B_{1g}, \text{non-loc}}$  (c),  $\chi_{pd}^{B_{1g}, \text{non-loc}}$  (d). These non-local terms appear to dominate the qualitative behavior of the Raman intensity shown in Fig. 5. (a) First and second nearest neighbor contributions add up in the paramagnetic state but subtract in the magnetic state while in (b) they almost cancel in the paramagnetic state but add up in the magnetic state. As a result, since  $I_M^\lambda$  is proportional to  $\chi_M^\lambda$  squared,  $I_{\alpha}^{A_{1g}}$  decreases in the magnetic state while  $I_{pd}^{A_{1g}}$  increases (Fig. 5). (d) In the magnetic state the contributions mostly add up but cancel at high values of  $U$  for  $\chi_{pd}^{B_{1g}, \text{non-loc}}$  which does not happen in (c), explaining the behavior of  $I_M^{B_{1g}}$  with  $U$ . Same parameters as in Fig. 5.

$U$ ,  $q_M^\lambda$  is strongly dependent on the parameters.

## B. Phonon self-energy

Fig. 7 shows the contributions of the electron-phonon couplings to the renormalization of the phonon frequency and to the phonon scattering rate as a function of  $U$  (see Section II C). To better visualize the variations of the phonon frequency and phonon broadening when entering in the magnetic state, we plot  $\Delta\Omega_M = \Pi'_M(\Omega_0, U) - \Pi'_M(\Omega_0, U=0)$  in Fig. 7 (a) and  $\Delta\Gamma_M = \Gamma_M(U) - \Gamma_M(U=0) = -(\Pi''_M(\Omega_0, U) - \Pi''_M(\Omega_0, U=0))$  in Fig. 7 (b).

When entering into the magnetic state ( $U \geq 1.45$  eV), both  $\Delta\Omega_\alpha$  (black) and  $\Delta\Omega_{pd}$  (red) are negative, resulting in phonon softening. This non-intuitive behavior is linked

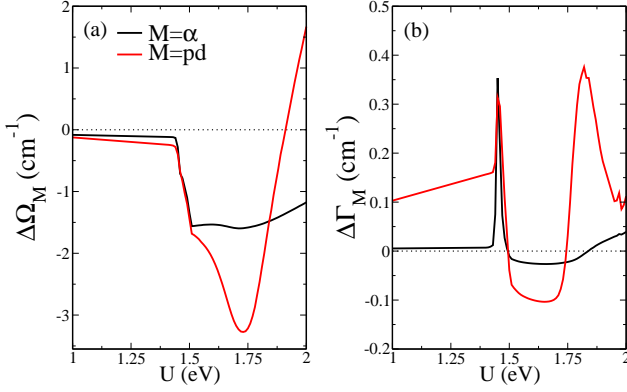


FIG. 7: (Color online) Renormalization of the phonon frequency  $\Delta\Omega_M = \Pi'_M(\Omega_0, U) - \Pi'_M(\Omega_0, U=0)$  (a) and phonon broadening  $\Delta\Gamma_M = -(\Pi''_M(\Omega_0, U) - \Pi''_M(\Omega_0, U=0))$  (b), for the electron-phonon couplings  $\hat{g}^\alpha$  and  $\hat{g}^{pd}$ .  $J_H/U = 0.25$ ,  $\Omega_0 = 20$  meV,  $\delta h = 0.02$  Å and a  $\delta$ -function broadening  $\eta = 3$  meV have been used.

to the multi-band character of the iron pnictides. Since  $\Pi'_M(\Omega)$  is the Kramers-Kronig integral of  $\Pi''_M(\Omega)$ , the softening is related to the spectral weight redistribution from high energies ( $\Omega > \Omega_0$ ) to lower energies ( $\Omega < \Omega_0$ ) when entering into the magnetic state. In one band models when a gap opens there is a shift of the spectral weight to higher energies and hardening is expected. Due to the multiorbital character of the iron superconductors, the reorganization of the low-energy spectral weight is non trivial and part of the spectra shifts closer to the Fermi energy, see for example Fig. 3 in Ref. [59].  $\Delta\Omega_\alpha$  is negative in all the range of parameters studied. On the contrary, the non-monotonic behavior of  $\Delta\Omega_{pd}$  results in hardening for  $U > 1.9$  eV. The different behavior due to  $\hat{g}^{pd}$  and  $\hat{g}^\alpha$  couplings at large values of  $U$  is associated with the different way in which the parameters  $|g_{nn'}^M|^2$  weight the energy excitations around  $\Omega_0$  in Eqs. (21) and (22).

As shown in Fig. 7 (b),  $\Delta\Gamma_\alpha$  and  $\Delta\Gamma_{pd}$  as a function of  $U$  are non-monotonic. They change considerably when entering into the magnetic state. Narrowing (broadening) of the phonon linewidth corresponds to negative (positive)  $\Delta\Gamma_M$ . The large peak at the onset of magnetism at  $U = 1.45$  eV is due to a particular band structure reorganization and is not a robust feature for other parameters. For larger interactions, the linewidth shows non-monotonic behavior: with narrowing followed by broadening.

#### IV. DISCUSSION AND COMPARISON TO EXPERIMENTS

Here we discuss our results in comparison with experiment. Note that we address the onset of the magnetic state as a function of the interaction  $U$  at zero temper-

ature, while in an experiment the varying parameter is the temperature and the interaction  $U$  remains constant. Experimentally, the  $A_{1g}$  As-phonon appears in the  $A_{1g}$  polarization symmetry in the paramagnetic state as a small or non-identifiable peak,<sup>1,8,42,43</sup> depending on the compound. This peak is strongly enhanced in 122 compounds when decreasing the temperature through the magneto-structural transition.<sup>1,3,8,42</sup> No phonon peak is observed because of symmetry in the  $B_{1g}$  polarization geometry in the paramagnetic state whereas a phonon anomaly clearly emerges in the magnetic phase.<sup>8,42,43,64</sup> In BaFe<sub>2</sub>As<sub>2</sub> the  $B_{1g}$  intensity is larger than the one corresponding to the  $A_{1g}$  polarization symmetry.<sup>8,42</sup> No peaks are observed in the  $B_{2g}$  symmetry in either state. Our calculations reproduce the appearance of a peak in the  $B_{1g}$  Raman polarization and not in the  $B_{2g}$  one in the anisotropic magnetic state without invoking the structural transition. As discussed in the previous section, this is a consequence of symmetry and not specific to any particular electron-phonon coupling. For the same reason no Raman signal is obtained in any of these symmetries  $B_{1g}$  and  $B_{2g}$  in the paramagnetic tetragonal state.

Whereas the appearance or not of an  $A_{1g}$  As-phonon peak in the different polarization geometries is quite simple, being dictated by pure group theory arguments, the quantitative discussion of the relative intensities is trickier. Each of the couplings here considered,  $\hat{g}^\alpha$  and  $\hat{g}^{pd}$ , accounts for one of the features observed experimentally but none of them alone can explain both. The coupling via  $\hat{g}^\alpha$  results, for interactions  $U > 1.8$  eV, in a larger intensity in the  $B_{1g}$  Raman polarization with respect to the  $A_{1g}$  one, as observed experimentally in BaFe<sub>2</sub>As<sub>2</sub>.<sup>8,42</sup> However, this behavior is accompanied by a reduction of the maximum intensity in the  $A_{1g}$  polarization symmetry by an order of magnitude in the magnetic state. This is at odds with the strong enhancement of the  $A_{1g}$  peak intensity experimentally observed in 122 compounds.<sup>1,3,8,42</sup> An increase of  $A_{1g}$  is observed with the coupling  $\hat{g}^{pd}$  but with  $I^{A_{1g}} \gg I^{B_{1g}}$ .

With the estimated couplings,  $\hat{g}^{pd}$  would dominate the Raman response and  $I^{A_{1g}} > I^{B_{1g}}$  would be expected (see Fig. 5). However, as discussed in Section II A, the exact dependence of the energy integrals on the As position  $f(R)$  is not known. The  $1/R^4$  function used is valid for localized orbitals and could strongly overestimate the electron-phonon coupling in a covalent system such as the iron pnictides. A more realistic functional dependence  $f(R)$ , with a slower dependence on  $R$ , or a difference in the distance dependence of  $pd\sigma$  and  $pd\pi$  could result in a dominance of  $\hat{g}^\alpha$  with  $I^{B_{1g}} > I^{A_{1g}}$ . However, note that the relation between magnetization and the system geometry resulting from LDA calculations,<sup>16</sup> with an increase of the magnetization for elongated tetrahedra, would be consistent with a dominance of the  $pd$ -dependence on the hoppings, while if they are modified according to the  $\alpha$ -dependence, the magnetization decreases (see Fig. 7 in Ref. [46]).

Experimentally,<sup>8</sup> the phonon lineshape of undoped

compounds has been found to be strongly symmetric with a Fano factor  $|q|$  bigger than 30. With electron doping it acquires an asymmetric shape, with  $q \sim -6.5$ . The experimental result in undoped pnictides is in agreement with the values of  $q_M$  obtained above in the orbital differentiation region. With electron doping we expect to enter into the itinerant region, in which the Fano factor is extremely sensitive to parameters and no robust prediction can be made.

Both hardening and softening of the  $A_{1g}$  As-phonon have been found in experiments when entering into the magnetic state,<sup>1,39,41</sup> with changes in the phonon frequency of the order of  $1-3 \text{ cm}^{-1}$  with respect to the zero temperature value. Both electron-phonon coupling and phonon-phonon interaction are expected to contribute to the frequency renormalization, but it is not obvious how to separate the two contributions. Our calculations report softening with frequency renormalizations of the same order of magnitude as experimentally found, except in the case of  $\hat{g}^{pd}$  coupling at large on-site interactions  $U$  which shows hardening.

Raman experiments have also reported a narrowing of the phonon linewidth which, depending on the material, ranges from  $1$  to  $3 \text{ cm}^{-1}$  when undergoing a magnetic transition.<sup>1,39,41</sup> For different on-site interactions, our calculations show both narrowing and broadening, but with a change in linewidth smaller than observed experimentally. The largest values are associated with the electron-phonon coupling channel  $\hat{g}^{pd}$ . The scattering rate is also very sensitive to the broadening parameter  $\eta$ , related to the electron scattering rate which is reduced in the magnetic state.

Our results show several features compatible with experimental reports but do not offer a completely satisfactory description of the experiments. It is not clear to us whether the discrepancies arise from the approximations done in the calculations (Hartree-Fock description of interactions and magnetism, neglect of the resonant Raman diagrams, lack of a self-consistent treatment of magnetization and phonons on an equal footing, or the coupling constants estimates) or whether electron-phonon couplings beyond those discussed here should be considered. Some of these electron-phonon couplings are (a) the dependence of the Coulombic crystal field  $\epsilon_\mu^{Coul}$  on the As position, (b) the dependence of the electronic interaction parameter  $U$  on the As-position due to the change in the screening<sup>65</sup> or (c) the spin-phonon coupling.<sup>5,21</sup>

## V. SUMMARY

In summary, in this paper we have calculated the Raman spectral properties of the optical out-of-plane As lattice vibrations (the  $A_{1g}$  As-phonon) in the paramagnetic and in the  $(\pi, 0)$  magnetic states of the iron pnictides. Using a tight binding Hamiltonian<sup>24</sup> based on the Slater-Koster approach, we have identified two qualitatively different sources of electron-phonon coupling: one

related to the Fe-As-Fe angle  $\alpha$  ( $\hat{g}^\alpha$ ), and one related to the Fe-As energy integrals  $pd\sigma$  and  $pd\pi$  ( $\hat{g}^{pd}$ ). Both of them contain a *local* ( $\mathbf{k}$  independent) term and a *non-local* ( $\mathbf{k}$  dependent) term, associated with the phonon modulation of the atomic Fe energy levels and with the effective Fe-Fe hopping amplitudes, respectively. The magnetic order has been taken into account by means of a mean-field Hartree-Fock of the electronic Hamiltonian.<sup>45,46</sup> The Raman response of the  $A_{1g}$  As-phonon has been calculated using a suitable generalization of the charge-phonon theory<sup>47</sup> to the Raman scattering.<sup>48,49</sup>

Our results indicate that a finite Raman intensity can be observed in the magnetic state in the  $B_{1g}$  but not in the  $B_{2g}$  polarization and it is a consequence of the coupling of the phonons to an anisotropic electronic state with non-equivalent  $x$  and  $y$  directions. Electron-phonon coupling via  $\hat{g}^\alpha$  can result in a Raman signal larger in the  $B_{1g}$  symmetry than in the  $A_{1g}$  symmetry, as observed experimentally in  $\text{BaFe}_2\text{As}_2$ . On the other hand, with  $\hat{g}^\alpha$  coupling the  $A_{1g}$  Raman intensity strongly decreases in the magnetic state, contrary to the experimental results. Coupling via  $\hat{g}^{pd}$  produces the opposite behavior: a very large enhancement of the  $A_{1g}$  intensity in the magnetic state, which stays much larger than the  $B_{1g}$  intensity in all the range of parameters studied. Due to uncertainties in the absolute values of the couplings, it is neither possible to know the intensity resulting from the sum of both  $\hat{g}^\alpha$  and  $\hat{g}^{pd}$  nor to address careful comparison with experiments.

For most values of the electronic interactions, the electron-phonon coupling induces softening of the phonon frequency in the magnetic state as compared to the paramagnetic state. This behavior is ascribed to the multi-orbital character of the iron superconductors. Hardening is observed for large values of the interaction  $U$  when coupling happens via  $\hat{g}^{pd}$ . Narrowing or broadening of the phonon line can appear in the magnetic state depending on the parameters.

With symmetry arguments similar to the ones used above, a finite phonon intensity in the  $B_{1g}$  symmetry would be also expected in a nematic state<sup>66,67</sup> in the absence of magnetism.<sup>68</sup> We also predict that in the double stripe magnetic state of FeTe, with non-equivalent diagonals, the out-of-plane  $A_{1g}$  Te-phonon acquires a finite Raman intensity in the  $B_{2g}$  polarization geometry, but not in the  $B_{1g}$  symmetry. It would be interesting to explore these possibilities experimentally.

We thank Yann Gallais for useful discussions and for sharing unpublished data with us. We have also benefited from conversations with Thomas Frederiksen, Jorge Iñiguez, Lex Kemper, Indranil Paul and Félix Yndurain. We acknowledge funding from MINECO-Spain through Grants FIS2008-00124, FIS2009-08744, FIS2011-29689 and FIS2012-33521. S.C. acknowledges support from Spanish Education Ministry programme SAB2010-0107. E.C. acknowledges support from the European FP7 Marie Curie project PIEF-GA-2009-251904 and Italian Project PRIN “GRAF” n. 20105ZZTSE.



## Appendix A

The local terms of the electron-phonon couplings  $\hat{g}^{\alpha,\text{loc}}$  and  $\hat{g}^{pd,\text{loc}}$  are calculated from the derivatives of the crystal field terms  $\epsilon_{\mu}^{\text{ind}}$  corresponding to virtual Fe-As forth and back transitions, see Eqs. (5) and (7). The expressions for these terms are calculated to second order in perturbation theory as detailed in Ref. [24] and are given here

$$\epsilon_{xy,xy}^{\text{ind}} = \frac{1}{|\epsilon_p - \epsilon_d|} \left[ \frac{1}{2} \cos^2 \alpha (4pd\pi^2(\cos(2\alpha) - 1) - 3pd\sigma^2(\cos(2\alpha) + 1)) \right], \quad (\text{A1})$$

$$\epsilon_{yz,yz}^{\text{ind}} = \epsilon_{zx,zx}^{\text{ind}} = \frac{1}{|\epsilon_p - \epsilon_d|} \left[ pd\pi^2(\cos(2\alpha) - \cos(4\alpha) - 2) + \frac{3}{4}pd\sigma^2(\cos(4\alpha) - 1) \right], \quad (\text{A2})$$

$$\epsilon_{3z^2-r^2,3z^2-r^2}^{\text{ind}} = \frac{1}{|\epsilon_p - \epsilon_d|} \left[ \frac{3}{2}pd\pi^2(\cos(4\alpha) - 1) + pd\sigma^2(12\cos(2\alpha) - 9\cos(4\alpha) - 11)/8 \right], \quad (\text{A3})$$

$$\epsilon_{x^2-y^2,x^2-y^2}^{\text{ind}} = \frac{1}{|\epsilon_p - \epsilon_d|} [-4pd\pi^2 \cos^2(\alpha)]. \quad (\text{A4})$$

$\epsilon_p$  and  $\epsilon_d$  are the onsite energies for the As p-orbitals and for the Fe d orbitals.  $\alpha$  is the angle formed by the Fe-As bond and the Fe-plane, see Fig. 1.  $pd\sigma$  and  $pd\pi$  are the energy integrals with values  $pd\sigma^2/(\epsilon_d - \epsilon_p) \approx 1$  eV and  $pd\pi/pd\sigma = -0.5$  respectively.

- 
- <sup>1</sup> K.-Y. Choi, D. Wulferding, P. Lemmens, N. Ni, S. L. Bud'ko, and P. C. Canfield, Phys. Rev. B **78**, 212503 (2008).
  - <sup>2</sup> M. Le Tacon, T. R. Forrest, C. Rüegg, A. Bosak, A. C. Walters, R. Mittal, H. M. Rønnow, N. D. Zhigadlo, S. Karpinski, et al., Phys. Rev. B **80**, 220504 (2009).
  - <sup>3</sup> L. Chauviere, Y. Gallais, M. Cazayous, and A. Sacuto, Phys. Rev. B **80**, 094504 (2009).
  - <sup>4</sup> A. Akrap, J. J. Tu, L. J. Li, G. H. Cao, Z. A. Xu, and C. C. Homes, Phys. Rev. B **80**, 180502 (2009).
  - <sup>5</sup> L. Zhang, P. Guan, D. Feng, X. Chen, S. Xie, and M. Chen, Journ. Am. Chem. Soc. **132**, 15223 (2010).
  - <sup>6</sup> A. A. Schafgans, B. C. Pursley, A. D. LaForge, A. S. Sefat, D. Mandrus, and D. N. Basov, Phys. Rev. B **84**, 052501 (2011).
  - <sup>7</sup> M. Nakajima, T. Liang, S. Ishida, Y. Tomioka, K. Kihou, C. H. Lee, A. Iyo, H. Eisaki, T. Kakeshita, T. Ito, et al., PNAS **108**, 12238 (2011).
  - <sup>8</sup> L. Chauvière, Y. Gallais, M. Cazayous, M. Méasson, A. Sacuto, D. Colson, and A. Forget, Phys. Rev. B **84**, 104508 (2011).
  - <sup>9</sup> T. Yildirim, Physica C: Superconductivity **469**, 42 (2009).
  - <sup>10</sup> L. Boeri, M. Calandra, I. I. Mazin, O. V. Dolgov, and F. Mauri, Phys. Rev. B **82**, 020506 (2010).
  - <sup>11</sup> M. Zbiri, H. Schober, M. R. Johnson, S. Rols, R. Mittal, Y. Su, M. Rotter, and D. Johrendt, Phys. Rev. B **79**, 064511 (2009).
  - <sup>12</sup> D. Reznik, K. Lokshin, D. C. Mitchell, D. Parshall, W. Dmowski, D. Lamago, R. Heid, K.-P. Bohnen, A. S. Sefat, M. A. McGuire, et al., Phys. Rev. B **80**, 214534 (2009).
  - <sup>13</sup> S. Hahn, Y. Lee, N. Ni, P. D. Canfield, A. I. Goldman, R. J. McQueeney, B. N. Harmon, A. Alatas, B. N. Leu, E. E. Alp, et al., Phys. Rev. B **79**, 220511 (2009).
  - <sup>14</sup> R. Mittal, M. K. Gupta, S. L. Chaplot, M. Zbiri, S. Rols, H. Schober, Y. Su, T. Brueckel, and T. Wolf, Phys. Rev. B **87**, 184502 (2013).
  - <sup>15</sup> S. Hahn, G. Tucker, J.-Q. Yan, A. Said, B. Leu, R. McCallum, E. Alp, T. Lograsso, R. McQueeney, and B. Harmon, Phys. Rev. B **87**, 104518 (2013).
  - <sup>16</sup> F. Yndurain and J. M. Soler, Phys. Rev. B **79**, 134506 (2009).
  - <sup>17</sup> M. Zbiri, R. Mittal, S. Rols, Y. Su, Y. Xiao, H. Schober, S. Chaplot, M. Johnson, T. Chatterji, Y. Inoue, et al., J. Phys.: Condens. Matter **22**, 315701 (2010).
  - <sup>18</sup> G. Q. Huang, Z. W. Xing, and D. Y. Xing, Phys. Rev. B **82**, 014511 (2010).
  - <sup>19</sup> B. Li, Z. Xing, and M. Liu, Appl. Phys. Lett. **98**, 072506 (2011).
  - <sup>20</sup> B. Li, Z. Xing, G. Huang, and M. Liu, J. Appl. Phys. **111**, 033922 (2012).
  - <sup>21</sup> T. Egami, B. Fine, D. Parshall, A. Subedi, and D. Singh, Adv. in Cond. Matt. Phys. **2010**, 164916 (2010).
  - <sup>22</sup> C. Gadermaier, V. V. Kabanov, A. S. Alexandrov, L. Stojchevska, T. Mertelj, C. Manzoni, G. Cerullo, N. D. Zhigadlo, J. Karpinski, Y. Q. Cai, et al., arXiv:1205.4978 (2012).
  - <sup>23</sup> V. Vildosola, L. Pourovskii, R. Arita, S. Biermann, and A. Georges, Phys. Rev. B **130**, 064518 (2008).
  - <sup>24</sup> M. J. Calderón, B. Valenzuela, and E. Bascones, Phys. Rev. B **80**, 094531 (2009).
  - <sup>25</sup> Z. P. Yin, S. Lebègue, M. J. Han, B. P. Neal, S. Y. Savrasov, and W. E. Pickett, Physical Review Letters **101**, 047001 (2008).
  - <sup>26</sup> F. Yndurain, European Physics Letters **94**, 37001 (2011).
  - <sup>27</sup> C. de la Cruz, W. Z. Hu, S. Li, Q. Huang, J. W. Lynn, M. A. Green, G. F. Chen, N. L. Wang, H. A. Mook, Q. Si, et al., Phys. Rev. Lett. **104**, 017204 (2010).
  - <sup>28</sup> C. H. Lee, A. Iyo, H. Eisaki, H. Kito, M. T. Fernandez-Diaz, T. Ito, K. Kihou, H. Matsuhata, M. Braden, and

- K. Yamada, J. Phys. Soc. Jpn. **77**, 083704 (2008).
- <sup>29</sup> J. Zhao, Q. Huang, C. de la Cruz, S. Li, J. Lynn, Y. Chen, M. Green, G. Chen, G. Li, Z. Li, et al., Nature Materials **7**, 953 (2008).
  - <sup>30</sup> K. Kuroki, H. Usui, S. Onari, R. Arita, and H. Aoki, Phys. Rev. B **79**, 224511 (2009).
  - <sup>31</sup> G. Garbarino, R. Weht, A. Sow, C. Lacroix, A. Sulpice, M. Mezouar, X. Zhu, F. Han, H. Hu Wen, and M. Núñez Regueiro, EPL **96**, 57002 (2011).
  - <sup>32</sup> K. W. Kim, A. Pashkin, H. Schfer, M. Beyer, M. Porer, T. Wolf, C. Bernhard, J. Demsar, R. Huber, and A. Leitenstorfer, Nature Materials **11**, 497 (2012).
  - <sup>33</sup> S. Kumar, L. Harnagea, S. Wurmehl, B. Buchner, and A. Sood, Eur. Phys. Lett. **100**, 57007 (2012).
  - <sup>34</sup> I. Avigo, R. Cortés, L. Rettig, S. Thirupathaiah, H. Jeevan, P. Gegenwart, T. Wolf, M. Ligges, M. Wolf, J. Fink, et al., J. Phys.: Condens. Matter **25**, 094003 (2013).
  - <sup>35</sup> L. Rettig, R. Cortés, J. H.S., P. Gegenwart, T. Wolf, J. Fink, and U. Bovenspiesen, arXiv:1304.5355v1 (2013).
  - <sup>36</sup> Z. K. Liu, R.-H. He, D. H. Lu, M. Yi, Y. L. Chen, M. Hashimoto, R. G. Moore, S.-K. Mo, E. A. Nowadnick, J. Hu, et al., Phys. Rev. Lett. **110**, 037003 (2013).
  - <sup>37</sup> V. Hadjiev, M. Iliev, K. Sasmal, Y.-Y. Sun, and C. Chu, Phys. Rev. B **77**, 220505R (2008).
  - <sup>38</sup> A. Litvinchuk, V. Hadjiev, M. Iliev, B. Lv, A. Guloy, and C. Chu, Phys. Rev. B **78**, 060503R (2008).
  - <sup>39</sup> Y. Gallais, A. Sacuto, M. Cazayous, P. Cheng, L. Fang, and H. Wen, Phys. Rev. B **78**, 132509 (2008).
  - <sup>40</sup> Y. Zhang, B. Zhou, F. Chen, J. Wei, M. Xu, L. Yang, C. Fang, W. Tsai, G. H. Cao, Z. A. Xu, et al. (2009), arXiv:0904.4022.
  - <sup>41</sup> M. Rahlenbeck, G. L. Sun, D. L. Sun, C. T. Lin, B. Keimer, and C. Ulrich, Phys. Rev. B **80**, 064509 (2009).
  - <sup>42</sup> S. Sugai, Y. Mizuno, R. Watanabe, T. Kawaguchi, K. Takenaka, H. Ikuta, Y. Takayanagi, N. Hayamizu, and Y. Sone, J. Phys. Soc. Jpn. **81**, 024718 (2012).
  - <sup>43</sup> A. M. Zhang and Q. M. Zhang, Mod. Phys. Lett. B **26**, 1230020 (2012).
  - <sup>44</sup> V. Gnezdilov, Y. Pashkevich, P. Lemmens, D. Wulferding, T. Shevtsova, A. Gusev, D. Chareev, and A. Vasiliev, Phys. Rev. B **87**, 144508 (2013).
  - <sup>45</sup> E. Bascones, M. J. Calderón, and B. Valenzuela, Phys. Rev. Lett. **104**, 227201 (2010).
  - <sup>46</sup> E. Bascones, B. Valenzuela, and M. J. Calderón, Phys. Rev. B **86**, 174508 (2012).
  - <sup>47</sup> M. J. Rice, Phys. Rev. Lett. **37**, 36 (1976).
  - <sup>48</sup> E. Cappelluti, L. Benfatto, and A. B. Kuzmenko, Phys. Rev. B **82**, 041402 (2010).
  - <sup>49</sup> E. Cappelluti, L. Benfatto, M. Manzardo, and A. B. Kuzmenko, Phys. Rev. B **86**, 115439 (2012).
  - <sup>50</sup> J. Slater and G. Koster, Phys. Rev. **94**, 1498 (1954).
  - <sup>51</sup> W. Harrison, *Elementary Electronic Structure* (World Scientific, Revised Edition, 2004).
  - <sup>52</sup> M. J. Calderón, G. Leon, B. Valenzuela, and E. Bascones, Phys. Rev. B **86**, 104514 (2012).
  - <sup>53</sup> T. Yoshida, S. Ideta, I. Nishi, A. Fujimori, M. Yi, R. G. Moore, S. K. Mo, D.-H. Lu, Z.-X. Shen, Z. Hussain, et al. (2012), arXiv:1205.6911.
  - <sup>54</sup> T. Sudayama, Y. Wakisaka, T. Mizokawa, S. Ibuka, R. Morinaga, T. J. Sato, M. Arita, H. Namatame, M. Taniguchi, and N. Saini (2012), arXiv:1206.2985.
  - <sup>55</sup> H. Ishida and A. Liebsch, Phys. Rev. B **81**, 054513 (2010).
  - <sup>56</sup> M. Aichhorn, S. Biermann, T. Miyake, A. Georges, and M. Imada, Phys. Rev. B **82**, 064504 (2010).
  - <sup>57</sup> Z. P. Yin, K. Haule, and G. Kotliar, Nature Physics **7**, 294 (2011).
  - <sup>58</sup> R. Yu and Q. Si (2012), arXiv:1202.6115.
  - <sup>59</sup> B. Valenzuela, M. J. Calderón, G. León, and E. Bascones, Phys. Rev. B **87**, 075136 (2013).
  - <sup>60</sup> T. Devereaux and R. Hackl, Rev. Mod. Phys. **79**, 175 (2007).
  - <sup>61</sup> G. D. Mahan, *Many-particle physics* (Plenum Publisher, New York, Third Edition, 2000).
  - <sup>62</sup> D. Lu, M. yi, S.-K. Mo, A. Erickson, J. Analytis, J.-H. Chu, D. Singh, Z. Hussain, T. Geballe, I. Fisher, et al., Nature **455**, 81 (2008).
  - <sup>63</sup> The symmetry of the electron-phonon system determines whether  $I_M^\lambda$  is finite or zero.  $B_{1g}$  and  $B_{2g}$  symmetries are orthogonal to the  $A_{1g}$  phonon symmetry in a tetragonal state. As a consequence,  $I_M^{B_{1g}}$  and  $I_M^{B_{2g}}$  vanish in the paramagnetic state (with tetragonal symmetry).
  - <sup>64</sup> S. Sugai, Y. Mizuno, R. Watanabe, T. Kawaguchi, K. Takenaka, H. Ikuta, Y. Takayanagi, N. Hayamizu, and Y. Sone, arXiv:1010.6151 (2010).
  - <sup>65</sup> G. Sawatzky, I. Elfimov, J. van den Brink, and J. Zaanen, Eur. Phys. Lett. **86**, 17006 (2009).
  - <sup>66</sup> C. Fang, H. Yao, W.-F. Tsai, J. Hu, and S. A. Kivelson, Phys. Rev. B **77**, 224509 (2008).
  - <sup>67</sup> R. M. Fernandes, A. V. Chubukov, J. Knolle, I. Eremin, and J. Schmalian, Phys. Rev. B **85**, 024534 (2012).
  - <sup>68</sup> A different contribution to the Raman spectrum in a nematic state has been studied in Ref. 69.
  - <sup>69</sup> H. Yamase and R. Zeyher, arXiv:1306.4267v1 (2013).